Thermal Analysis of an Induction Motor Using MATLAB.

Dr. -Ing. O. I. Okoro

Department of Electrical Engineering, University of Nigeria, Nsukka, Enugu State, Nigeria.
Email: ogbonnayaokoro@hotmail.com

ABSTRACT

The paper uses a commercial software package, MATLAB® to investigate the estimation of induction motor average temperatures within different parts. A thermal network model is developed and the resulting algebraic and differential systems of equations solved in order to determine the thermal behaviour of the test machine under steady and transient conditions, respectively. It is observed that the computed mean steady state temperatures of the machine parts at No-Load, Rated Load and Blocked Rotor operations compare satisfactorily well with the measured steady state temperatures.

(Key words: thermal behaviour, squirrel cage induction machine, no load, rated load, blocked rotor)

INTRODUCTION

The most important features of a squirrel cage induction machine that enhances its suitability in hostile environment are ruggedness and robustness[1]. However, when the machine is continuously operated on load, it may be necessary to monitor the temperature of the various parts of the machine if the aforementioned important features are not to be compromised due to excessive heating. Generally, when the thermal limit of an electrical machine is exceeded, the following undesirable effects result[2]: Loss of dielectrical property of the insulating material, thermal bending of the rotor and consequent loss of eccentricity, bearing wear and vibration, deterioration of bearing lubricants and thermal stresses and changes in geometry of the machine elements due to thermal expansion. In order to predict the temperatures in electrical machines, thermal models are used. Thermal models of electrical machines vary in degree of complexities depending on areas of applications and the level of accuracy to which the models are expected to give when compared to the physical temperature measurements of the test machine. Most thermal models are based on the similarity between Ohm's law of electrical conduction and Fourier's law of heat conduction. The lumped-parameter (Thermal network) models and the Finite-Element Method, FEM [3,4], are the most frequently used thermal models. In this paper, a thermal network model is used to estimate the temperatures of the 7.5 KW test machine. The theory of thermal network model is first presented; followed by losses calculation and background information on heat transfer. The paper also presents the developed thermal model for the test machine. The experimental verifications and computer simulation are discussed together with concluding comments.

THERMAL NETWORK MODEL THEORY

In a thermal network model, it is assumed that all the heat generation in the component is concentrated in one point—usually referred as the node. A node connotes the mean temperature of the component. In a thermal network model as shown in Figure 1, each node is assigned a thermal capacitance, C_{th} and heat flowing between nodes and represented as current source, P_G is passed through thermal resistance, R_{th}. Thermal network models as applicable to electrical machines range from one dimensional to three dimensional. However, a two dimensional or three dimensional thermal network model can be developed by connecting several one-dimensional models together in the point of the mean temperature. A detailed analysis on this principle is given by Mellor [3].

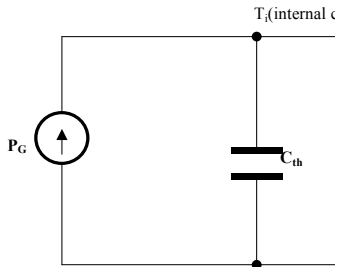

Figure 1: Thermal network model.

For small induction machines, the machine elements are represented by the temperature rise with the ambient air temperature taken as

a thermal reference. The heat generation, P_G as in electrical machines represents the losses in the machine parts (e.g. Stator, Rotor, etc). The thermal capacitance,C_{th} of an element is usually calculated from the geometry and material data of the element. It is expressed as,

$$C_{th} = \rho C_p V \qquad \textbf{(1)}$$

Where, V = volume of the element, ρ = material density, C_p = specific heat capacity of the material.

The thermal capacitancies of the test machine elements calculated using equation (1) are shown in Appendix A. Thermal network models offer both steady and transient states solutions for the temperature difference between the element and the ambient air temperature. The general transient equation for a thermal network with n nodes and each linked to the others through thermal resistances, R_{ij} is expressed thus:

$$C_i \frac{d\theta_i}{dt} = P_i - \sum_{j=1}^{n} \frac{\theta_i - \theta_j}{R_{ij}} \qquad \textbf{(2)}$$

Where, I = 1….n, C_i = node thermal capacitance, θ_i = node temperature rise, R_{ij} = thermal resistance between adjoining nodes i, j, P_i = heat generation at node i. In matrix form, equation (2) can be expressed as:

$$\frac{d\theta_t}{dt} = [\mathbf{C}_t]^{-1}[\mathbf{P}_t] - [\mathbf{C}_t]^{-1}[\mathbf{G}_t][\boldsymbol{\theta}_t] \qquad \textbf{(3)}$$

Where the thermal capacitance matrix $(\mathbf{C}_t)$, the loss matrix $(\mathbf{P}_t)$, the temperature rise matrix $(\boldsymbol{\theta}_t)$ and the conductance matrix $(\mathbf{G}_t)$ are defined as,

$$[\mathbf{C}_t] = \begin{bmatrix} C_1 & 0 & 0 & - & - & - & 0 \\ 0 & C_2 & 0 & - & - & - & 0 \\ 0 & 0 & C_3 & - & - & - & 0 \\ - & - & - & - & - & - & - \\ - & - & - & - & - & - & - \\ - & - & - & - & - & - & - \\ 0 & 0 & 0 & 0 & 0 & 0 & C_n \end{bmatrix} \qquad \textbf{(4)}$$

$$[\mathbf{P}_t] = [P_1 \quad P_2 \quad P_3 \quad - \quad - \quad - \quad P_n]^t \qquad \textbf{(5)}$$

$$[\theta_t] = [\theta_1 \quad \theta_2 \quad \theta_3 \quad - \quad - \quad - \quad \theta_n]^t \qquad \textbf{(6)}$$

$$[\mathbf{G}_t] = \begin{bmatrix} \sum_{i=1}^{n} G_{1,i} & -G_{1,2} & -G_{1,3} & - & - & - & -G_{1,n} \\ -G_{2,1} & \sum_{i=1}^{n} G_{2,i} & -G_{2,3} & - & - & - & -G_{2,n} \\ -G_{3,1} & -G_{3,2} & \sum_{i=1}^{n} G_{3,i} & - & - & - & -G_{3,n} \\ - & - & - & - & - & - & - \\ - & - & - & - & - & - & - \\ - & - & - & - & - & - & - \\ -G_{n,1} & -G_{n,2} & -G_{n,3} & - & - & - & \sum_{i=1}^{n} G_{n,i} \end{bmatrix} \qquad \textbf{(7)}$$

In equation (7),

$G_{1,i} = \frac{1}{R_{1,i}}$,etc Also due to symmetry, $G_{1,2}$ = $G_{2,1}$ and $G_{1,3}$ = $G_{3,1}$ etc.

Under steady-state conditions, the thermal capacitance can be considered at full capacity $\left[\frac{d\theta_i}{dt} = 0\right]$, and therefore disappears from the transient state equation. By so doing, equation (8) results,

$$P_i = \sum_{j=1}^{n} \frac{\theta_i - \theta_j}{R_{i,j}} \qquad i = 1….n \qquad \textbf{(8)}$$

In matrix form, equation (8) becomes,

$$[\mathbf{P}_t] = [\mathbf{G}_t][\boldsymbol{\theta}_t] \qquad \textbf{(9)}$$

and

$$[\boldsymbol{\theta}_t] = [\mathbf{G}_t]^{-1}[\mathbf{P}_t] \qquad \textbf{(10)}$$

CALCULATION OF LOSSES

Consideration of losses in induction machines is important not only in the determination of the machine's efficiency, but also in the heating of the machine and hence the rating or the obtainable power output without undue deterioration of the insulation. Losses in induction machines can be broadly classified into: Ohmic losses, Iron losses, Mechanical losses, and Additional losses.

Ohmic losses are load losses emanating from currents flowing through the stator and rotor windings. Iron losses consist of the eddy current losses and hysteresis losses. Iron losses are dependent on the machine's flux which in turn is almost proportional to voltage.

Mechanical losses are often referred to as friction and windage losses, and consist of brush and bearing friction, windage, and the power required to circulate the air through the induction machine and ventilating system, if one is available.

Additional losses in induction machines can be treated as stray losses. These losses are due to the non-uniform current distribution in the copper and the additional core losses produced in the iron by distortion of the magnetic flux by the load current. In this paper, the stray load losses, which represent about 1.8% of the machine rated power as reported by [5], are taken into consideration and added to the rotor losses. The test machine power losses at No-Load, Rated Load and Blocked Rotor operations at 50 Hz were calculated by a program based on finite-element analysis (FEA) of electromagnetic fields [6]. The distributions of these losses are presented in Figures 2, 3, and 4 for the various operating conditions.

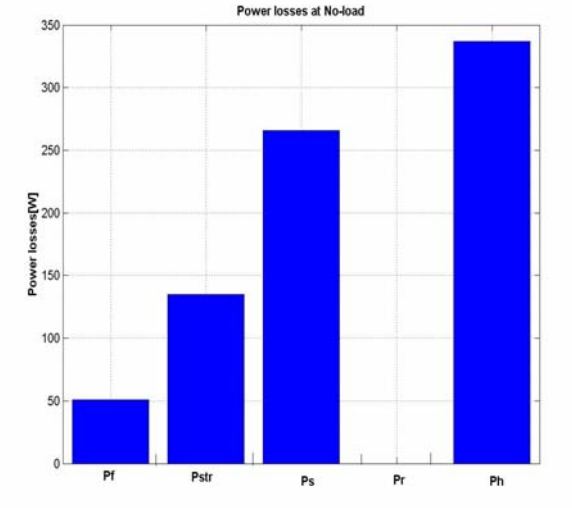

Figure 2: Power losses of the 7.5KW motor at No-load.

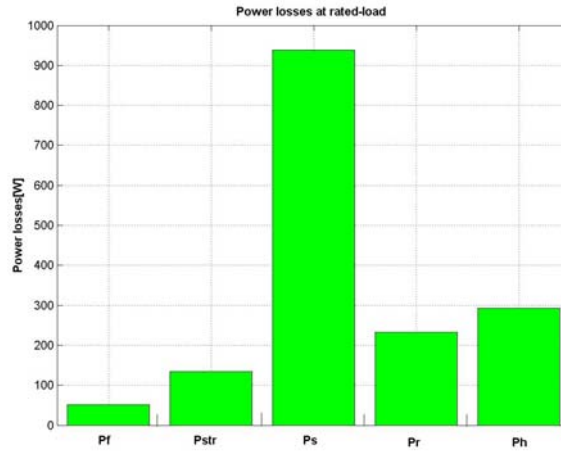

Figure3: Power losses of the 7.5KW motor at rated load.

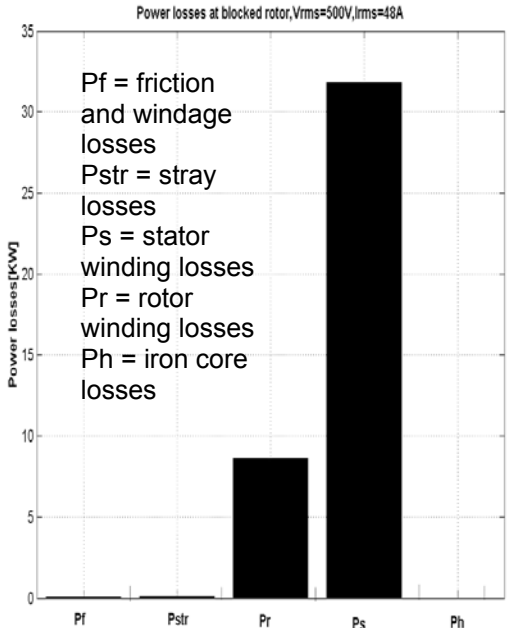

Figure 4:. Power losses of the 7.5KW motor at blocked rotor.

HEAT TRANSFER THEORY

In order to calculate the thermal resistances of a thermal network, a background knowledge of heat transfer is appropriate. Three modes of heat transfer are considered for the calculation of the thermal resistances: Conduction, Convection and Radiation.

The general equation governing heat conduction in rectangular co-ordinate system (x,y,z) is given by [7]:

$$\frac{1}{\alpha}\frac{\partial\theta}{\partial t}=\frac{\partial^2\theta}{\partial x^2}+\frac{\partial^2\theta}{\partial y^2}+\frac{\partial^2\theta}{\partial z^2}+\frac{1}{K}Q \qquad \textbf{(11)}$$

and

$$\alpha=\frac{K}{\rho c_p} \qquad \textbf{(12)}$$

Where, c_p equals the specific heat of the material,[J/(Kg.°C)], Q = heat generation rate, [W/m^3], ρ = density of material,[kg/m^3], K = thermal conductivity, [W/(m.°C)], θ = temperature, [°C]

For one-dimensional analysis, which is applied in this work, the general expression for the conductive heat transfer is given by Fourier's law as:

$$q=-K\frac{\partial\theta}{\partial x} \qquad \textbf{(13)}$$

where, q= heat flux, [W/m^2], x= distance,[m]

Therefore, the thermal resistance between two points becomes,

$$R_{th} = \frac{x_2 - x_1}{kA} \qquad \textbf{(14)}$$

Where A is the cross-sectional area,[m^2]. Heat transfer as a result of convection is described by:

$$q = h_c\left(\theta_w - \theta_f\right) \qquad \textbf{(15)}$$

Where, θ_w = the temperature of the surface and θ_f = the temperature at a distant point from the surface. The coefficient of heat transfer, h_c is dependent on the nature of flow (laminar or turbulent), the body geometry, the average temperature and physical characteristics of the fluid, the nature of the heat transfer (natural or forced). The thermal resistance due to convection is estimated by:

$$R_{th} = \frac{1}{h_c A} \qquad \textbf{(16)}$$

The net heat transfer by radiation between two real bodies is derived from the Stefan Boltzmann's law and given by [7] as,

$$q_r = A_1\varepsilon_1\delta\left(\theta_w^4 - \theta_f^4\right) \qquad \textbf{(17)}$$

where, A_1 = area of surface one, ε_1 = emissivity of surface one, $\left[0 \le \varepsilon \le 1\right]$. For Iron, ε =0.96 and for Aluminium, ε =0.08. δ = Stefan-Boltzmann constant, [5.6697x10^{-8} W/(m^2.K^4)]. The thermal resistance to the surroundings due to radiation is given by:

$$R_{th} = \frac{\theta_w - \theta_f}{A_1\varepsilon_1\delta\left(\theta_w^4 - \theta_f^4\right)} \qquad \textbf{(18)}$$

The heat transfer mechanism in the 7.5 KW Squirrel-cage induction machine is shown in Figure 5.

The thermal resistances of the test machine elements were calculated using the various heat transfer mode formula are shown in Appendix A.

MATHEMATICAL REPRESENTATIONS OF THE DEVELOPED THERMAL MODEL

The thermal network model for the squirrel-cage induction machine is developed according to the principles reported by

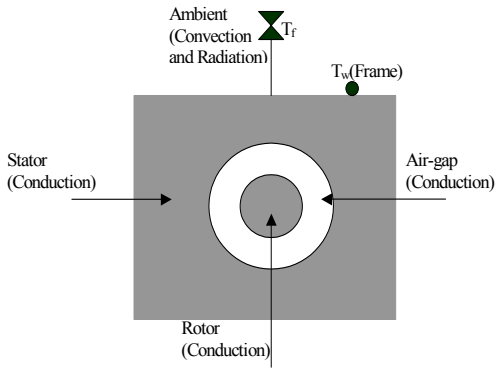

Figure 5: Squirrel-cage induction machine heat transfer mechanism.

Kessler [8]. Figure 6 shows the typical construction of a Squirrel-Cage induction machine.

In developing the thermal network model, the machine geometry is divided into basic elements and each element being identified by a node in the thermal network with its corresponding thermal capacitance and heat source. The developed thermal network model is shown in Figure 7. The model consists of 11 nodes and 15 thermal resistances.

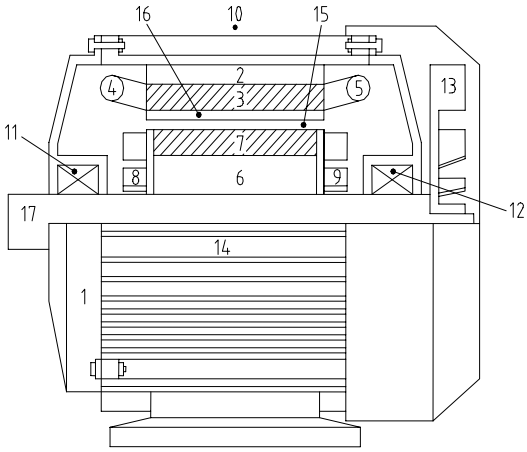

1. Frame. 2. Stator iron. 3.Stator winding. 4.,5. End windings. 6. Rotor iron. 7. Rotor winding. 8..9. Endrings. 10. Ambient air. 11.,12. Bearing. 13. Fan. 14. Cooling ribs. 15. Air gap. 16. Stator teeth. 17. Shaft

Figure 6: Typical Construction of Squirrel-Cage Induction Machine.

TRANSIENT STATE THERMAL MODEL EQUATIONS

The transient thermal network equation presented above is used to develop the transient state thermal model equations for the induction machine thermal model of Figure 7.

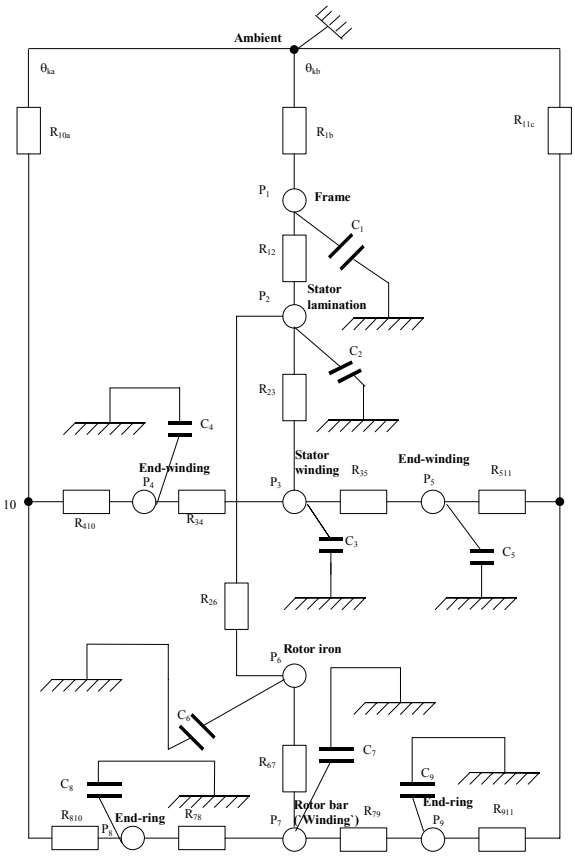

Figure 7: Thermal network model representation for the 7.5KW induction machine

$$\begin{bmatrix} \dot{\theta}_1 \\ \dot{\theta}_2 \\ \dot{\theta}_3 \\ \dot{\theta}_4 \\ \dot{\theta}_5 \\ \dot{\theta}_6 \\ \dot{\theta}_7 \\ \dot{\theta}_8 \\ \dot{\theta}_9 \\ \dot{\theta}_{10} \\ \dot{\theta}_{11} \end{bmatrix} = \begin{bmatrix} C_1 & 0 & 0 & 0 & 0 & 0 & 0 & 0 & 0 & 0 & 0 \\ 0 & C_2 & 0 & 0 & 0 & 0 & 0 & 0 & 0 & 0 & 0 \\ 0 & 0 & C_3 & 0 & 0 & 0 & 0 & 0 & 0 & 0 & 0 \\ 0 & 0 & 0 & C_4 & 0 & 0 & 0 & 0 & 0 & 0 & 0 \\ 0 & 0 & 0 & 0 & C_5 & 0 & 0 & 0 & 0 & 0 & 0 \\ 0 & 0 & 0 & 0 & 0 & C_6 & 0 & 0 & 0 & 0 & 0 \\ 0 & 0 & 0 & 0 & 0 & 0 & C_7 & 0 & 0 & 0 & 0 \\ 0 & 0 & 0 & 0 & 0 & 0 & 0 & C_8 & 0 & 0 & 0 \\ 0 & 0 & 0 & 0 & 0 & 0 & 0 & 0 & C_9 & 0 & 0 \\ 0 & 0 & 0 & 0 & 0 & 0 & 0 & 0 & 0 & C_{10} & 0 \\ 0 & 0 & 0 & 0 & 0 & 0 & 0 & 0 & 0 & 0 & C_{11} \end{bmatrix}^{-1} \begin{bmatrix} P_1+\theta_{kb}*G_{1b} \\ P_2 \\ P_3 \\ P_4 \\ P_5 \\ P_6 \\ P_7 \\ P_8 \\ P_9 \\ \theta_{ka}*G_{10a} \\ \theta_{kc}*G_{11c} \end{bmatrix} - [\mathbf{C}]^{-1} * [\boldsymbol{\theta}] + [\mathbf{P}]$$

$\mathbf{C_t}$ $\mathbf{P_t}$

$$\begin{bmatrix} G_{11} & -G_{12} & 0 & 0 & 0 & 0 & 0 & 0 & 0 & 0 & 0 \\ -G_{21} & G_{22} & -G_{23} & 0 & 0 & -G_{26} & 0 & 0 & 0 & 0 & 0 \\ 0 & -G_{32} & G_{33} & -G_{34} & -G_{35} & 0 & 0 & 0 & 0 & 0 & 0 \\ 0 & 0 & -G_{43} & G_{44} & 0 & 0 & 0 & 0 & 0 & -G_{410} & 0 \\ 0 & 0 & -G_{53} & 0 & G_{55} & 0 & 0 & 0 & 0 & 0 & -G_{511} \\ 0 & -G_{62} & 0 & 0 & 0 & G_{66} & -G_{67} & 0 & 0 & 0 & 0 \\ 0 & 0 & 0 & 0 & 0 & -G_{76} & G_{77} & -G_{78} & -G_{79} & 0 & 0 \\ 0 & 0 & 0 & 0 & 0 & 0 & -G_{87} & G_{88} & 0 & -G_{810} & 0 \\ 0 & 0 & 0 & 0 & 0 & 0 & -G_{97} & 0 & G_{99} & 0 & -G_{911} \\ 0 & 0 & 0 & -G_{104} & 0 & 0 & 0 & -G_{108} & 0 & G_{1010} & 0 \\ 0 & 0 & 0 & 0 & -G_{115} & 0 & 0 & 0 & -G_{119} & 0 & G_{1111} \end{bmatrix} \begin{bmatrix} \theta_1 \\ \theta_2 \\ \theta_3 \\ \theta_4 \\ \theta_5 \\ \theta_6 \\ \theta_7 \\ \theta_8 \\ \theta_9 \\ \theta_{10} \\ \theta_{11} \end{bmatrix} \quad \textbf{(19)}$$

$\mathbf{G_t}$ $\boldsymbol{\theta_t}$

The transient state equations taken node by node and written in state variable form give:

The enteries of the $\mathbf{G_t}$-matrix are defined as in equations (20a-20k). θ_{ka}, θ_{kb} and θ_{kc} are the ambient temperatures and are assumed to be constant.

$G_{11} = G_{1b}+G_{12}$ **(20a)**
$G_{22} = G_{21}+G_{23}+G_{26}$ **(20b)**
$G_{33} = G_{32}+G_{35}+G_{34}$ **(20c)**
$G_{44} = G_{43}+G_{410}$ **(20d)**
$G_{55} = G_{53}+G_{511}$ **(20e)**
$G_{66} = G_{62}+G_{67}$ **(20f)**
$G_{77} = G_{78}+G_{79}+G_{76}$ **(20g)**
$G_{88} = G_{87}+G_{810}$ **(20h)**
$G_{99} = G_{97}+G_{911}$ **(20i)**
$G_{1010}=G_{104}+G_{10a}+G_{108}$ **(20j)**
$G_{1111}=G_{115}+G_{11c}+G_{119}$ **(20k)**

STEADY-STATE THERMAL MODEL EQUATIONS

Generally, as shown above, the algebraic steady-state temperature rise in a thermal network is given by:

$$[\boldsymbol{\theta}_t] = [\mathbf{G}_t]^{-1}[\mathbf{P}_t] \quad \textbf{(21)}$$

The variables $\boldsymbol{\theta}_t$,$\mathbf{G_t}$ and $\mathbf{P}_t$ have been defined previously in section 2. Applying equation (21) to the developed thermal network model of figure 7 the following expressions result:

$$[\mathbf{P}_t] = [P_1+\theta_{kb}G_{1b} \quad P_2 \quad P_3 \quad P_4 \quad P_5 \quad P_6 \quad P_7 \quad P_8 \quad P_9 \quad \theta_{ka}G_{10a} \quad \theta_{kc}G_{11c}]^t \quad \textbf{(22a)}$$

$$[\boldsymbol{\theta}_t] = [\theta_1 \quad \theta_2 \quad \theta_3 \quad \theta_4 \quad \theta_5 \quad \theta_6 \quad \theta_7 \quad \theta_8 \quad \theta_9 \quad \theta_{10} \quad \theta_{11}]^t \quad \textbf{(22b)}$$

$$[\mathbf{G}_1]=\begin{bmatrix} G_{11} & -G_{12} & 0 & 0 & 0 & 0 & 0 & 0 & 0 & 0 & 0 \\ -G_{21} & G_{22} & -G_{23} & 0 & 0 & -G_{26} & 0 & 0 & 0 & 0 & 0 \\ 0 & -G_{32} & G_{33} & -G_{34} & -G_{35} & 0 & 0 & 0 & 0 & 0 & 0 \\ 0 & 0 & -G_{43} & G_{44} & 0 & 0 & 0 & 0 & 0 & -G_{410} & 0 \\ 0 & 0 & -G_{53} & 0 & G_{55} & 0 & 0 & 0 & 0 & 0 & -G_{511} \\ 0 & -G_{62} & 0 & 0 & 0 & G_{66} & -G_{67} & 0 & 0 & 0 & 0 \\ 0 & 0 & 0 & 0 & 0 & -G_{76} & G_{77} & -G_{78} & -G_{79} & 0 & 0 \\ 0 & 0 & 0 & 0 & 0 & 0 & -G_{87} & G_{88} & 0 & -G_{810} & 0 \\ 0 & 0 & 0 & 0 & 0 & 0 & -G_{97} & 0 & G_{99} & 0 & -G_{911} \\ 0 & 0 & 0 & -G_{104} & 0 & 0 & 0 & -G_{108} & 0 & G_{1010} & 0 \\ 0 & 0 & 0 & 0 & -G_{115} & 0 & 0 & 0 & -G_{119} & 0 & G_{1111} \end{bmatrix} \quad \textbf{(22c)}$$

EXPERIMENTAL VERIFICATIONS

Temperature measurements on the test machine were carried out at No-Load, Rated Load and Blocked Rotor operations. Iron-constantan, usually called Type J thermocouples, were used for the measurements. These types of thermocouples are very popular due to their high Seebeck coefficient and low price. The main demerit of thermocouples is their relatively weak signal which makes their reading sensitive to corruption from electrical signal. During blocked rotor operation, 12 and 20 thermoelements were installed in the stator and rotor parts of the test machine respectively as shown in Figure 8 and Figure 9.

Figure 8: Stator part of the test machine showing the installed J-type thermoelements.

All the thermocouples were connected to a 32-channel programmable recorder (see label E in Figure 10) which combines the functions of a recorder with that of a datalogger and a data acquisition system. Measuring signals are printed with the built-in-inkjet printer on paper as values(with date and time). The time interval between print-outs is selectable. The

Figure 9: Rotor part of the test machine showing the installed J-type thermoelements.

print-out shows the physical units of the measuring values, for example degree Centigrade. Through the built-in RS232 interface, the measured data can be sent to a connected computer (See label F in Figure 10). The computer stores and evaluates the measured data. The RS232 interface can transmit up to 40 values per second per channel. During the Blocked Rotor operation, the machine was star-connected and its rotor blocked. A 500 V rms voltage was supplied to the machine with a stator current of 48 A for about 9 s and the temperature readings of the thermocouples recorded for every one second interval. It was observed that some of the thermocouples stopped working, probably because the soldering loosened.

The set-up for the No-Load and Rated Load operations is as shown in Figure 10. At No-Load operation, the machine was delta-connected with a rated voltage of 340 V.

The machine was allowed to run at No-Load for two hours until thermal equilibrium was attained. Temperature readings for every two minutes interval was recorded. It is important to add that only the temperatures of the stator parts were recorded since the rotor parts were inaccessible during motor operation. The steady-state temperature of the drive side end-ring was however measured with the help of Infra-red instrument two hours after the machine has reached thermal equilibrium. The Load test was carried out the same way as the No-Load test but with the machine operated at rated full load until thermal equilibrium was reached. Measurements were recorded for every two minutes intervals. In both operations, the air flow rate into the test

machine was kept constant and measured with the help of Anemometer (See label B in Figure 10). The results of the steady-state measurements are presented in this paper. The report on the results of the transient state measurements is in progress and will soon be published.

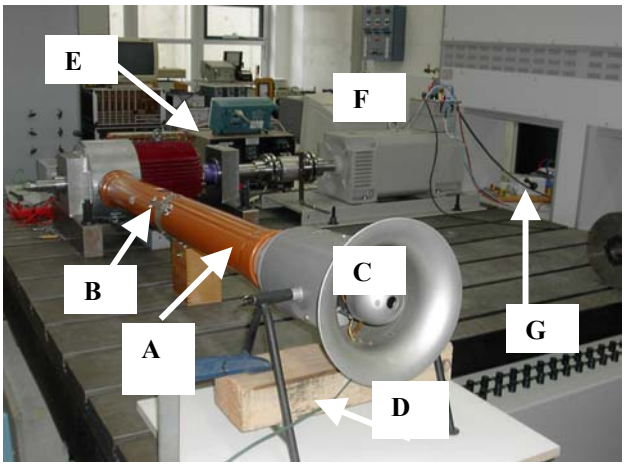

Air channel pipe(A), Anemometer On-Off switch(B), Ventilator(C), Leads to the voltage regulator(D), 32-channel programmable recorder(E), Computer(F), Star-Delta switch(G).

Figure 10: Experimental set-up for the heat runs at No-load and rated load operations.

COMPUTER SIMULATION AND RESULTS

The developed thermal model gives rise to a set of algebraic and differential equations which describe the thermal behaviour of the machine under steady and transient conditions respectively. MATLAB® m-files [9] are developed for half of the machine in order to determine the average temperature rise in the various parts of the machine. This reduces the set of differential equations to eight. Temperature rise of the machine parts is computed from the state equations using Runge-Kutta numerical method [10]. By incorporating the ambient temperature, rotor iron, rotor winding, end ring, stator lamination, frame, stator winding, and end winding temperatures under steady and transient conditions are then computed. Table 1, Table 2, and Table 3 show the computed and measured steady temperatures for the test machine at No-load, Rated Load, and Blocked Rotor conditions respectively. Figure 11, Figure 12, and Figure 13 show the simulated transient temperatures of the test machine under No-load, Rated Load, and Blocked Rotor operations respectively.

Model component	Predicted temperature [°C] (Steady state)	Measured temperature [°C] (Steady state)
Frame	40.12	44.80
Stator lamination	47.60	-
Stator winding	51.72	50.13
End winding	52.91	51.81
Rotor iron	53.04	-
Rotor winding	53.17	-
End ring	53.75	52.1*

Table 1: Measured and predicted steady state temperatures at No-load

Model component	Predicted temperature [°C] (Steady state)	Measured temperature [°C] (Steady state)
Frame	54.71	56.30
Stator lamination	67.60	-
Stator winding	82.96	82.13
End winding	91.26	85.93
Rotor iron	83.67	-
Rotor winding	84.12	-
End ring	88.30	84.5*

Table 2: Measured and predicted steady state temperatures at rated load

Model component	Predicted temperature [°C] (Steady state)	Measured temperature[°C] (Steady state)
Frame	24.41	23.1*
Stator iron	37.08	42.25
End winding	88.78	88.43
Rotor iron	30.94	-
Rotor winding	32.86	46.30
End ring	84.45	95.35

*** measurement done with the infra-red instrument.**

Table 3: Measured and predicted steady state temperatures at blocked rotor

CONCLUSIONS AND OBSERVATIONS

The steady state thermal measurements carried out on the test machine show that the proposed thermal network model is capable of predicting the mean temperatures in the test machine with reasonable accuracy during No-load, rated load and blocked rotor operations.

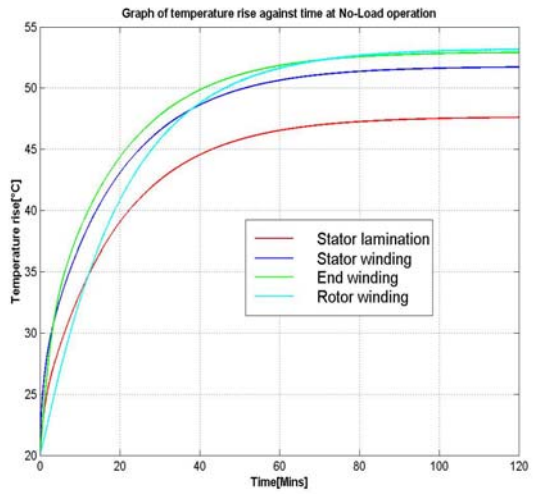

Figure 11a: Predicted temperatures at No-Load

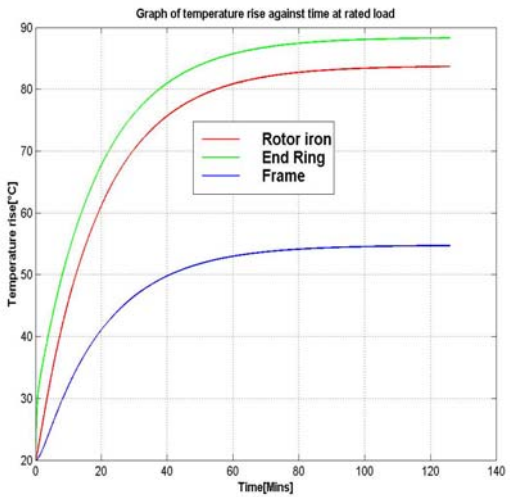

Figure 12b: Predicted temperatures at Rated Load

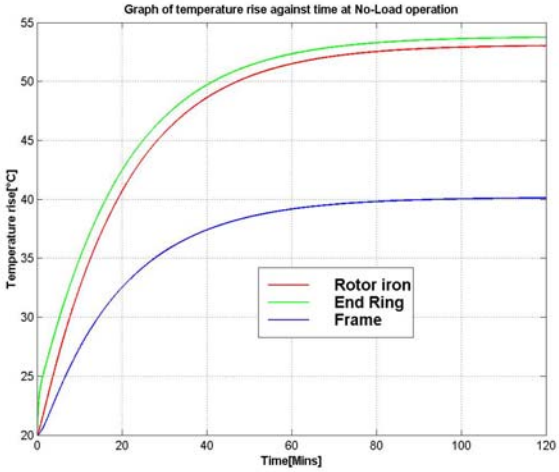

Figure 11b: Predicted temperatures at No-load

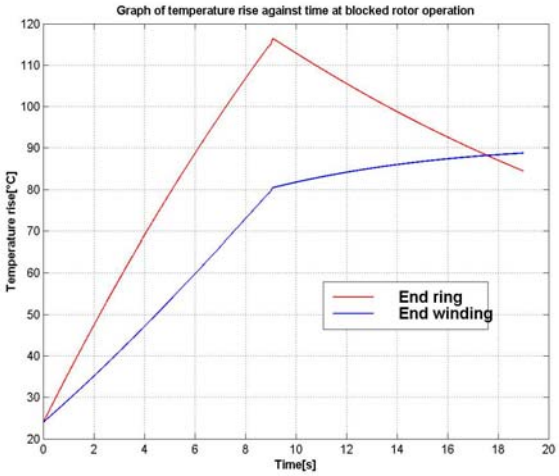

Figure 13a: Predicted temperatures at Blocked Rotor.

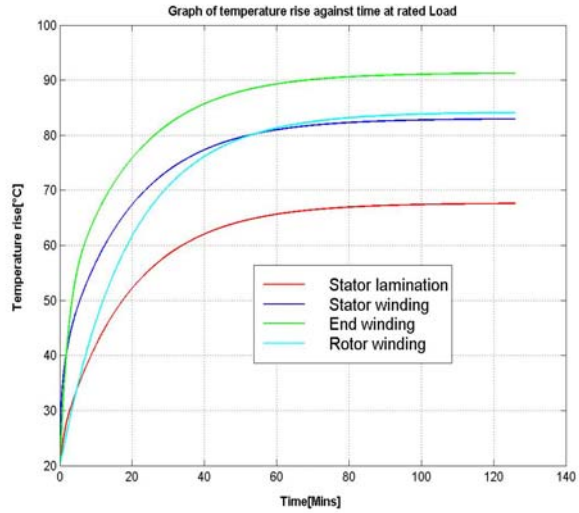

Figure 12a: Predicted temperatures at Rated Load

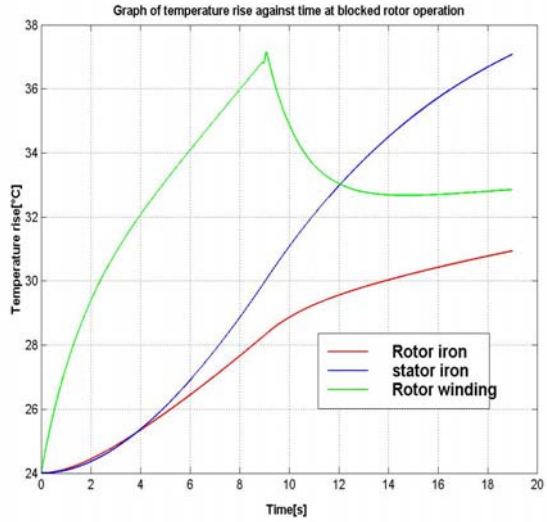

Figure 13b: Predicted temperatures at Blocked Rotor.

The errors observed between the measured and calculated mean steady state temperatures may be as a result of the fact that the developed thermal model calculates the average temperatures inside the stator and rotor windings, whereas the installed thermoelements measure only the outside temperature of the stator and rotor windings. Probable error may also be due to the errors emanating from the calculation of the model's thermal resistances and capacitances which are dependent on the material properties of the machine—to which accurate information from the manufacturer on same is highly necessary. These errors are, however, within acceptable limits for practical purposes. Therefore, this paper has shown that it is possible to accurately model the thermal behaviour of squirrel-cage induction machine at No-Load, Rated Load and Blocked-Rotor conditions using MATLAB®. The analysis and results presented in this paper will provide a useful insight into the allowable thermal limit of induction machine parts prior to operation.

REFERENCES

[1.] MacDonald, M.L. and Sen, P.C.: Control loop study of induction motor drives using D.Q. Model. Conference record of industry Applications Society. IEEE/IAS Annual Meeting, 1978.

[2.] Okoro, O.I.: Dynamic and Thermal Modelling of Induction Machine with Non-Linear Effects. Dissertation, University of Kassel, September 2002.

[3.] Mellor, P.H. et. al: Lumped parameter thermal model for electrical machines of TEFC design. *IEE Proc. B*, 138, (5), PP.205-218, 1995.

[4.] Griffith, J.W. et, al: Induction motor squirrel cage rotor winding thermal analysis. *IEEE Transactions on Energy Conversion*, Vol. EC-1, No.3, PP. 22-25, September 1986.

[5.] IEEE Standard Test Procedure for Polyphase Induction Motors and Generators, *IEEE Standard* 112-1991, 1991.

[6.] ANSOFT**:** Maxwell 2D/RMxprt FEA—Simulation Program. Ansoft Corporation, Munich.

[7.] Özisik, M. N.:*Heat Transfer—A basic Approach*. McGraw-Hill Book Company, New York, 1985.

[8.] Kessler, A.: Versuch einer genaueren Vorausberechnung des zeitlichen Erwärmungsverlaufes Elektrischer Maschinen mittels Wärmequellennetzen. *Archiv für Elektrotechnik*, Vol.45 No.1, PP.59-76, 1960.

[9.] The MATLAB compiler user's guide, in: *Mathworks Handbook*. Mathworks, April 1997.

[10.] Gerald,C.F. *Applied Numerical Analysis*. Addison-Wesley publishing company, London,1978.

APPENDIX A: CALCULATED THERMAL RESISTANCES AND CAPACITANCES

Thermal capacitances	Values [J/K]	Thermal resistances	Values [K/W]
C_1	18446.55	R_{1b}	0.0416
C_2	4450.625	R_{12}	15.44e-3
C_3	423.388	R_{23}	35.58e-3
C_4	539.92	R_{26}	0.135
C_5	3204.08	R_{35}	0.1751
C_6	408.267	R_{511}	1.886
C_7	218.785	R_{67}	4.115e-3
C_8	1006	R_{79}	0.1055
		R_{911}	0.932
		R_{11c}	0.015

ACKNOWLEDGEMENTS

The author wishes to express his thanks to DAAD for her financial support and to Prof. Dr.-Ing. B. Weidemann for his assistance and advice in producing this paper.

ABOUT THE AUTHOR

Dr.–Ing. O.I. Okoro holds a Ph.D. in Electrical Machines from the University of Kassel, Germany where he conducted his research under a DAAD Scholarship. He currently lectures in the Department of Electrical Engineering at the University of Nigeria, Nsukka. His research interests are in the areas of dynamic simulation and control of induction machines as well as in the thermal and dynamic analysis of AC machines. He is a member of the IEEE.

SUGGESTED CITATION

Okoro, O.I. 2003. Thermal Analysis of an Induction Motor Using MATLAB. *Greenwich Journal of Science and Technology*. 4(1):65-74.


Greenwich Journal of Science and Technology